Analytical Methods

ROYAL SOCIETY OF CHEMISTRY

PAPER

View Article Online
View Journal

Cite this: DOI: 10.1039/d0ay00575d

Flower-like Ag coated with molecularly imprinted polymers as a surface-enhanced Raman scattering substrate for the sensitive and selective detection of glibenclamide†

Xiaohui Ren and Xin Li *

Flower-like Ag was formed by nanosheet self-assembly as a SERS-active substrate and was utilized for the preparation of flower-like Ag@molecularly imprinted polymers (MIPs) as a surface-enhanced Raman scattering (SERS) sensor. Based on the combination of the molecular imprinting technique and SERS technology, the flower-like Ag@MIPs with high sensitivity and excellent selectivity were used as SERS substrates for the detection of glibenclamide. The imprinted layer could effectively protect the flower-like Ag from oxidation and thereby may improve the stability of the SERS substrate. The intensities of the characteristic peaks obtained for the flower-like Ag@MIPs were higher than that of flower-like Ag. By applying the flower-like Ag@MIPs as an efficient and ultra-sensitive SERS platform, glibenclamide was quantitatively detected in trace concentrations as low as 1 ng mL^{-1}. Furthermore, the SERS enhancement for the flower-like Ag@MIPs was due to the synergetic effect between electromagnetic enhancement and chemical enhancement. We believe that this reliable method can open up new opportunities for practical chemosensor or biosensor applications.

Received 20th March 2020
Accepted 8th May 2020

DOI: 10.1039/d0ay00575d

rsc.li/methods

Introduction

5-Chloro-*N*-[2-[4-[[[(cyclohexylamino)carbonyl]amino]sulphonyl]phenyl]ethyl]-2-methoxybenzamide, namely, glibenclamide is an oral sulfonylurea antidiabetic drug used for the treatment of type II diabetes.[1] It plays an important role in stimulating the pancreatic β-cells to release insulin and reduce the concentration of serum glucose.[2–4] Glibenclamide with satisfactory biomembrane permeability and poor water solubility is utilized as a class II drug to cure mild-to-moderate diet-uncontrolled patients. It is suitable for non-insulin-dependent diabetes mellitus in initiating diet treatment failure as compared to the first-generation sulphonylurea drugs.[4] However, the excessive use of glibenclamide may have different side effects on the pancreas and kidneys, such as weight gain, high hypoglycemic risk, postprandial hyperinsulinemia, and other complications or serious side effects.[5,6] The traditional methods used to detect the content of glibenclamide are commonly based on gas chromatography,[7] micellar electrokinetic chromatography with non-ionic surfactants,[8] and high-performance liquid chromatography with mass spectrometry or UV detection.[9,10] Nevertheless, these analysis methods have some disadvantages, such as a tedious sample pretreatment process, the need for professional technicians, and the use of large amounts of organic solvents. Therefore, there is an urgent need to develop a rapid and sensitive analytical method to investigate glibenclamide in blood, its pharmacokinetics, and some health products.

In recent decades, surface-enhanced Raman scattering (SERS) has attracted significant attention for rapidly detecting pollutants with high sensitivity and "fingerprint" properties.[11] The SERS enhancement is attributed to the combination of the electromagnetic mechanism (EM) with a main enhancement of 10^{-10}-fold and a chemical mechanism (CM) with an additional enhancement of 10^{-4}-fold.[12] Based on the EM and CM enhancements, SERS can achieve single-molecule detection.[13,14] At present, SERS is not only used in scientific research, but also used as a promising detection method in practical life, such as food safety,[15,16] environmental monitoring,[17,18] healthcare products,[19,20] and biomedical diagnosis.[21] In order to meet these requirements, researchers have developed many different types of SERS substrates.[22–24] Nevertheless, it is still a challenge to find a method that can realize ultra-sensitive detection and especially recognize analytes for social problems.

The molecularly imprinted technology, also known as the molecular template technology, refers to a specific target analyte as a template molecule to prepare a polymer with specific selectivity for the molecule.[25–27] This obtained polymer is called a molecularly imprinted polymer (MIP).[28] At present, MIPs have

MIIT Key Laboratory of Critical Materials Technology for New Energy Conversion and Storage, School of Chemistry and Chemical Engineering, Harbin Institute of Technology, Harbin 150001, China. E-mail: lixin@hit.edu.cn

† Electronic supplementary information (ESI) available. See DOI: 10.1039/d0ay00575d

attracted considerable attention because of their specific selectivity, strong resistance to harsh conditions and wide versatility.[29–31] Therefore, taking advantage of MIPs would promote the stability, sensitivity and selectivity of SERS signals. However, a lot of reports about the combination of SERS and MIPs focus on the detection of organic dyes,[32,33] endocrine disruptors,[34] agricultural residues,[35,36] disease diagnosis,[37,38] cancer imaging[39] and single-cell analysis.[40] For example, Gao and coworkers presented an innovative approach by combing MIPs and SERS for the detection of Sudan I and obtained $\sim 4 \times 10^4$ SERS enhancement.[32] The core–shell silver-MIP hybrid structure was also fabricated with high sensitivity and selectivity as the SERS substrate to detect rhodamine 6G.[24] The development of MIPs and SERS for the determination of chlorpyrifos was reported by Feng *et al.* and the MIPs-SERS sensor they obtained is more sensitive to detecting chlorpyrifos in apple juice.[35] Recently, the integration of MIPs and SERS was successfully applied in the detection of bisphenol A with the high selectivity of the MIPs, excellent sensitivity of Ag, and the low-cost preparation method.[41] Nevertheless, there is little or no literature on the combination of MIPs and SERS for the detection of antidiabetic drugs.

Herein, the flower-like Ag@MIPs were successfully prepared by using glibenclamide as the template molecule and acrylamide as the functional monomer. When compared with spherical or other common morphologies, the flower-like Ag fabricated by the nanosheets exhibited an advantage in SERS because the gap between the nanosheets can generate numerous enhanced SERS "hot spots". Therefore, the flower-like Ag was chosen as the SERS-active substrate. Based on the flower-like Ag, the flower-like Ag@MIPs with effective hot spots and excellent selectivity showed outstanding SERS performance. In addition, the flower-like Ag@MIPs have high sensitivity and good reusability of the template molecule due to the combination of SERS and MIPs. The minimum detection concentration of glibenclamide was as low as 1 ng mL^{-1}. The specific recognition and excellent selectivity of flower-like Ag@MIPs were investigated by making a comparison with flower-like Ag and detecting metformin hydrochloride, respectively. On the basis of the flower-like Ag@MIPs SERS sensor, a rapid, simple and efficient analytical method can be established to detect the safety of the medicine and health products.

Experimental section

Materials

Silver nitrate ($AgNO_3$), ascorbic acid, and acetonitrile were obtained from Sinopharm Chemical Reagent Co. Ltd. (Shanghai, China). Malonic acid and acrylamide were bought from the Tianjin Guangfu Fine Chemical Research Institute (Tianjin, China). Glibenclamide was purchased from J&K Chemical (Beijing, China). Metformin hydrochloride, 3-aminopropyltriethoxysilane (APTES), and ethylene glycol dimethacrylate (EGDMA) were obtained from Aladdin (Shanghai, China). Ethanol, methanol, and acetic acid were acquired from Tianjin Fuyu Fine Chemical Co. Ltd. (Tianjin, China). 2,2-Azobisisobutyronitrile (AIBN) was bought from Tianjin Kermel Chemical Reagent Co. Ltd. (Tianjin, China). High-purity water was obtained from a Milli-Q water system (Millipore, Billerica, MA, USA). All reagents utilized in this work were of analytical purity and were used without further treatment.

Apparatus

A scanning electron microscope (SEM) equipped with an energy dispersive spectrometer (EDS) and transmission electron microscope (TEM) was used to determine the morphologies of the prepared samples (SEM, Hitachi S-8010 and TEM, Tecnai G20, Philips). X-ray diffraction analysis (XRD, PANalytical B.V. X'Pert3 Powder) was used to record the crystalline phase of the prepared samples. Fourier transform infrared spectra (FT-IR, Avatar 360 Nicolet) were utilized to characterize the functional groups of the prepared samples. A Renishaw inVia micro-Raman spectrometer was applied to obtain the SERS spectra and SERS mapping (Renishaw, Britain).

Synthesis of flower-like Ag particles

The chemical reduction method was utilized to prepare the flower-like Ag particles. $AgNO_3$ (1.0 mmol) was dissolved in 1.0 mL deionized water to obtain the $AgNO_3$ aqueous solution, which was added to a beaker with 10.0 mL deionized water in an ice-water bath. Malonic acid (0.1 mL, 0.1 mol L^{-1}) was then injected into the above solution under stirring. After stirring for 10 min, the ascorbic acid (1.0 mL, 1.0 mol L^{-1}) was quickly poured into the reaction solution and stirred for another 15 min. The product was obtained by centrifugation (8000 rpm, 10 min), and washed several times with water and ethanol. The flower-like Ag particles were collected after drying under a vacuum.

Synthesis of the flower-like Ag@MIP hybrid

APTES was used to modify the surface of flower-like Ag particles, and 200 mg of flower-like Ag particles were dispersed in 20 mL ethanol by ultrasonication. After 15 min of ultrasonication, 2 mL of APTES was added to the above mixture, which was flooded with nitrogen, then the reaction mixture was stirred for 24 hours at 40 °C in an oil bath. The products were dried in a vacuum after washing several times with ethanol. The flower-like Ag@MIP hybrid was prepared by the following steps. Glibenclamide (0.1 mmol) was dissolved in ethanol (10.0 mL) and acetonitrile (10.0 mL) with ultrasonication until completely dissolved and then acrylamide (0.4 mmol) was added. After 10 min of ultrasound treatment, 200 mg of the above products (modified flower-like Ag particles) were put in the mixture solution with another 10 min of ultrasound treatment. The EGDMA (2 mmol) was injected into the above reaction mixture and then 20 mg of AIBN was added. After filling with nitrogen, the reaction liquid was stirred at 60 °C in an oil bath for 24 h. The template molecule was eluted by using methanol–acetic acid (9 : 1, v/v) until no glibenclamide was detected in the washing solution. The final product, the flower-like Ag@MIPs hybrid, was obtained after drying under vacuum.

Results and discussion

A detailed procedure for preparing flower-like Ag@MIPs is shown in Fig. 1A. First, the hierarchical flower-like Ag was synthesized by a low-cost and environment-friendly method in an ice-water bath, in which malonic acid acted as the guiding agent, and ascorbic acid was used as the reducing agent. APTES was then used to modify the flower-like Ag, and obtain the amino-modified flower-like Ag. Third, the flower-like Ag@MIPs were prepared by using surface imprinting.

The molecular electrostatic potential (MEP) of glibenclamide and acrylamide are shown in Fig. 1B. In the glibenclamide molecule, the four O-atoms (hydrogen acceptors) form hydrogen bonds with amino groups in acrylamide. Acrylamide was chosen as the functional monomer to interact with the template molecule glibenclamide by hydrogen bonds to form a pre-polymerization complex in the solvent of acetonitrile. The crosslinking agent plays an important role in forming the MIPs layer. Here, EGDMA was selected as the crosslinker due to its having a suitable solubility in acetonitrile. During the surface polymerization process, the active sites were formed through intermolecular hydrogen bonds instead of intra-molecular hydrogen bonds. Therefore, after the template molecules were eluted with methanol : acetic acid (9 : 1, v/v) solution, the active sites were left with specific recognition to the template molecule.

Characterization

In order to illustrate the morphology of the prepared materials, SEM images of the flower-like Ag and Ag@MIPs were obtained. As shown in Fig. 2A and B, the initial structure of the flower-like Ag showed uniform morphology, with the surface composed of irregular lamellar structures. Although the SEM images of the flower-like Ag@MIPs (Fig. 2C and D) were a little different from the flower-like Ag, the surface morphology of the flower-like Ag@MIPs was still spiky and sharp. According to the inset TEM images of Fig. 2B and D, the thickness of the imprinted layer was about 6–12 nm for the flower-like Ag@MIPs. Based on the SEM and TEM results, we concluded that the imprinted layer was successfully introduced on the surface of the flower-like Ag.

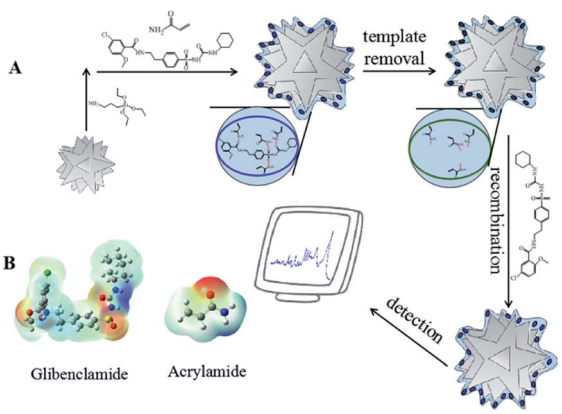

Fig. 1 Schematic illustration of the fabrication and detection process of flower-like Ag@MIPs (A), and the molecular electrostatic potential of glibenclamide and acrylamide (B).

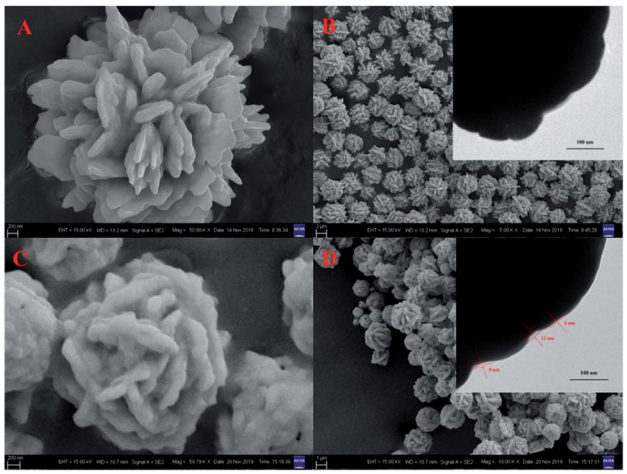

Fig. 2 SEM images of flower-like Ag (A and B), and Ag@MIPs (C and D). TEM images of flower-like Ag (inset of B) and Ag@MIPs (inset of D).

To further investigate the composition of the flower-like Ag and Ag@MIPs, EDS was used to characterize the chemical constituents of the prepared samples. Fig. 3 exhibits the images of flower-like Ag and Ag@MIPs obtained by EDS and EDS mapping. As shown in Fig. 3A, the EDS image of the flower-like Ag indicated the Ag and C elements. Compared with the EDS image of the flower-like Ag, the EDS image of the flower-like Ag@MIPs not only shows the Ag and C elements but also contains O and N elements. The N and O elements were bought about by the introduction of the imprinted layer. While the imprinted layer was very thin, the amounts of N and O elements were very low, which was similar to the results obtained by EDS mapping (Fig. 3C and D).

The phase information of the flower-like Ag and Ag@MIPs was characterized by XRD. Fig. 4A shows the XRD results of the flower-like Ag and distinctly demonstrates the highly crystallized structures. The five characteristic reflection peaks located at 38.25°, 44.43°, 64.60°, 77.54° and 81.70° are in agreement with (111), (200), (220), (311), and (222), which correspond to the face-centered cubic (fcc) structure standard JCPDS (no. 04-0783) data. The results indicate that the prepared flower-like Ag was not oxidized since the oxide diffraction peak of Ag did not appear. The reflection peak of the flower-like Ag at 38.25° was indexed to (111) of the bulk Ag. The stronger intensity peak at

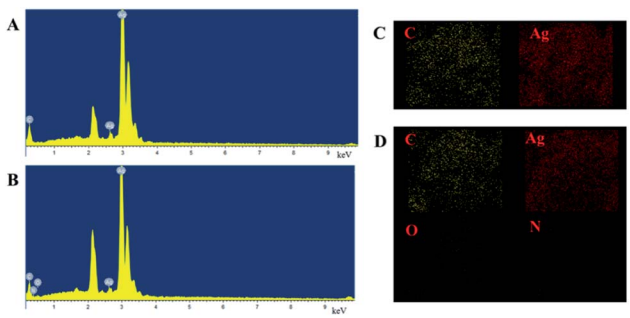

Fig. 3 The EDS images of flower-like Ag (A) and Ag@MIPs (B), and EDS mapping of flower-like Ag (C) and Ag@MIPs (D).

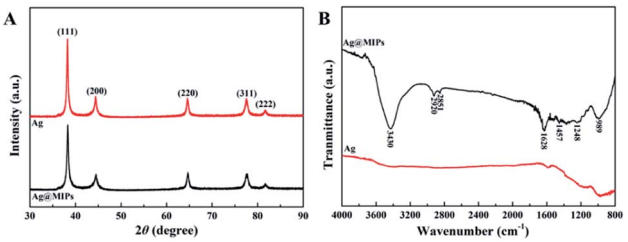

Fig. 4 XRD curves of flower-like Ag and Ag@MIPs (A), and the FT-IR curves of flower-like Ag and Ag@MIPs (B).

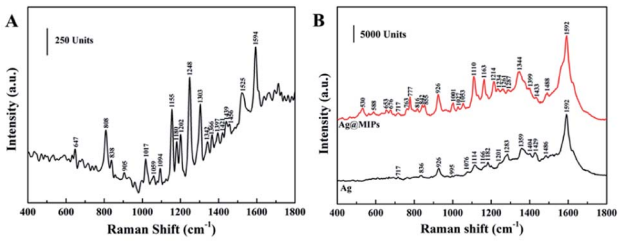

Fig. 5 The Raman spectrum of glibenclamide solid powder (A), and the SERS spectra of glibenclamide obtained from the flower-like Ag and Ag@MIPs (B).

38.25° indicated that the (111) facet was abundant and the flower-like Ag preferred to grow along the [111] direction. Meanwhile, results were also obtained from the intensity ratio value for (111)/(200), where (3.98) was bigger than the standard file value of (2.1).[42] Because the prepared samples consist of pure crystalline Ag, no other impurity peaks were shown in the XRD curve of flower-like Ag. Compared with the XRD curve of flower-like Ag, the flower-like Ag@MIPs had the same five reflection peaks at 2θ values of 38.34°, 44.51°, 64.69°, 77.54° and 81.70°. This shows that the introduction of the imprinted layer did not change the crystal structure of the inner flower-like Ag.

The prepared flower-like Ag and Ag@MIPs were also characterized by FT-IR spectroscopy. As shown in Fig. 4B, no obvious infrared peaks were observed on the curve of flower-like Ag. This indicates that flower-like Ag was completely washed in the cleaning process, and no ascorbic acid and malonic acid remained from the preparation process. However, some peaks were observed in the infrared spectrum of flower-like Ag@MIPs. The characteristic peak at 989 cm^{-1} was the C–H stretching vibration in vinyl. The symmetrical stretching vibration of C–O–C was located at 1248 cm^{-1}, which may be due to the participation of EGDMA in the polymerization. In addition, the weak peak at 1457 cm^{-1} belonged to the C–H stretching vibration in $–CH_2$. Furthermore, the C=O stretching vibration appeared at 1628 cm^{-1}, and there was an adsorption peak at 2851 cm^{-1}, which corresponded to the vibration of N–H on acrylamide. The characteristic peak at 2920 cm^{-1} was attributed to the C–H stretching vibration in $–CH_3$, and the strong peak at 3430 cm^{-1} corresponded to the N–H and/or O–H stretching vibration.

It can be concluded, therefore, that the imprinted layer was successfully introduced on the surface of flower-like Ag.

SERS performance of glibenclamide adsorbed on the flower-like Ag@MIPs

Glibenclamide, as the template molecule, was used to investigate the SERS performance of the prepared flower-like Ag@MIPs. As shown in Fig. 5A, the Raman spectrum was obtained from the solid powder of glibenclamide. The SERS spectra of glibenclamide are shown in Fig. 5B, and the Raman and SERS spectral assignment of glibenclamide are shown in Table 1. According to the SERS spectra, glibenclamide at a concentration of 500 μg mL^{-1} was acquired from flower-like Ag. More characteristic peaks appeared as compared to the Raman spectrum and this indicated that high-quality SERS spectra of glibenclamide were obtained. The SERS characteristic peak of glibenclamide molecules at 717 cm^{-1} was responsible for the associated in-plane deformation of the aromatic ring and SO_2 group. Moreover, the SERS band at 836 cm^{-1} was attributed to the NCN angular deformation and/or CC stretching vibration. The characteristic peak at around 995 cm^{-1} was assigned to the CO and/or HCNC deformation vibration. The fingerprint at 1114 cm^{-1} was ascribed to the deformation vibration of NC, CNC, and/or CCN. The prominent peak at 1166 cm^{-1} was attributed to the SO_2 symmetric stretching. The SERS peaks of HCN and HCC deformation vibrations were located at 1182 cm^{-1}, 1201 cm^{-1}, and 1283 cm^{-1}. The SERS band at 1429 cm^{-1} was assigned to deformation vibrations of the alkyl groups. The strong peak at 1592 cm^{-1} was attributed to the C=C stretching of the benzene ring. Fig. 5B shows that the SERS spectrum of glibenclamide at a concentration of 100 μg mL^{-1} was obtained from the flower-like Ag@MIPs. The characteristic SERS peaks at 530 cm^{-1}, 588 cm^{-1}, 653 cm^{-1}, 676 cm^{-1}, 717 cm^{-1}, 763 cm^{-1}, 777 cm^{-1}, 816 cm^{-1}, 842 cm^{-1}, 855 cm^{-1}, 926 cm^{-1}, 1001 cm^{-1}, 1027 cm^{-1}, 1053 cm^{-1}, 1110 cm^{-1}, 1163 cm^{-1}, 1214 cm^{-1}, 1234 cm^{-1}, 1261 cm^{-1}, 1287 cm^{-1}, 1344 cm^{-1}, 1399 cm^{-1}, 1433 cm^{-1}, 1488 cm^{-1} and 1587 cm^{-1} were consistent with the SERS spectra obtained from the flower-like Ag with a difference in strength or an offset in position. This is mainly due to the different action sites of SERS substrates, and there will be some differences even with the same action sites with different types of actions. Fig. 5B shows that the SERS peaks obtained from flower-like Ag@MIPs were stronger as compared to the flower-like Ag. This result demonstrated that the specific recognition sites ("hot spots") in the imprinted layer of flower-like Ag@MIPs could be more effective than the gaps between or in the flower-like Ag. The existence of the imprinted layer can not only protect the internal flower-like Ag oxidation, but can also provide an electromagnetic enhancement channel for the template molecule to come in contact with the plasmonic metal.

Concentration-dependent SERS spectra of glibenclamide

The concentration-dependent SERS spectra of glibenclamide were performed on flower-like Ag@MIPs substrates. The results are shown in Fig. 6A. The flower-like Ag@MIPs as the SERS substrate was utilized to investigate glibenclamide with the concentration range from 1 ng mL^{-1} to 100 μg mL^{-1}. With the decrease in the concentration of glibenclamide, the

Table 1 The Raman and SERS vibrational wavenumbers (in cm^{-1}) and assignments of glibenclamide

Solid powder	Flower-like Ag	Flower-like Ag@MIPs	Vibration type
		530	The deformation vibrations of the aromatic ring and SO_2 group
		588	
647		653	
		676	
	717	717	
		763	
		777	
808		816	The deformation vibrations of CCC or HCCC
838	836	842	The NCN angular deformation vibrations plus CC stretching vibrations
905		855	
	926	926	
1017	995	1001	The CO and/or HCNC deformation vibration
		1027	
1059	1076	1053	
1094	1114	1110	The angular deformations vibrations of NC, CNC, and/or CCN
1155	1166	1163	The SO_2 symmetric stretching vibrations
1180	1182	1214	The deformation vibrations of HCN and HCC
1202	1201	1234	
1248		1261	
1303	1283	1287	
1342	1359	1344	
1366			
1397	1404	1399	
1421			
1439	1429	1433	The deformation vibrations of the alkyl groups
1456	1486	1488	
1525			
1594	1592	1592	The C=C stretching vibrations of benzene ring

characteristic peaks obtained by flower-like Ag@MIPs were gradually weakened. Furthermore, the distinguishable SERS peaks were clearly seen even at concentrations as low as 1 ng mL^{-1} (Fig. 6C); therefore, the minimum detection limit of flower-like Ag@MIPs for glibenclamide can be below 1 ng mL^{-1}. Plots of SERS intensity were obtained as a function of the concentration of glibenclamide for the characteristic bands at 926 cm^{-1} and 1592 cm^{-1}, respectively (Fig. 6B). The linear relationship between the concentration of glibenclamide and the SERS intensity was realized in the range of 1 ng mL^{-1} to 100 μg mL^{-1}. At the low concentration, the SERS intensity was more correlated with the concentration of glibenclamide, which is due to the imprinting sites in the MIPs layer not being completely filled. However, at the high concentration, the SERS enhancement comes not only from the template molecules in the imprinted cavity, but also from the template molecules not adsorbed in the imprinted cavity.

The selectivity of flower-like Ag@MIPs

Specific recognition plays an important role in the performance research of MIPs. Thus, metformin hydrochloride was chosen for studying the specific recognition of flower-like Ag@MIPs. The imprinted cavities in the MIPs layer matched the size, shape and functional groups of the template molecules formed after eluting the template molecules. As shown in Fig. 6D, the flower-like Ag@MIPs exhibited the significant SERS signals for glibenclamide, while there were no SERS signals for metformin hydrochloride. This was mainly due to the imprinted layer of flower-like Ag@MIPs capturing the template molecules rather than the other molecules, even if they had a smaller structure. Compared with the flower-like Ag@MIPs, the flower-like Ag not

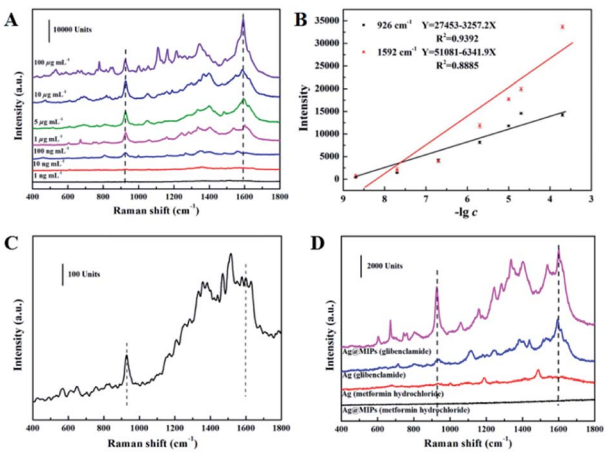

Fig. 6 Concentration-dependent SERS spectra of glibenclamide obtained from flower-like Ag@MIPs (A); the linear relationship of SERS intensity as a function of the glibenclamide concentration for the characteristic peaks at 926 cm^{-1} and 1592 cm^{-1} (B); the SERS spectrum of glibenclamide concentration at 1 ng mL^{-1} (C); the SERS spectra of flower-like Ag and Ag@MIPs in 1 μg mL^{-1} glibenclamide and metformin hydrochloride solution, respectively (D).

only had the SERS signals for glibenclamide, but also showed the characteristic peaks for metformin hydrochloride. A lot of specific active sites for glibenclamide were created at the imprinted layer of the flower-like Ag@MIPs. Although the molecular structure of metformin hydrochloride is smaller than that of glibenclamide, it is different from the functional group of the template molecule. Thus, metformin hydrochloride can get into the imprinted cavities, but the weak covalent and/or reversible covalent bond was very unstable, which may be the reason the SERS signal of metformin hydrochloride was not generated. Based on the above discussion, the flower-like Ag@MIPs have the specific recognition ability for the detection of glibenclamide.

Reusability of flower-like Ag@MIPs

The reusability of the SERS substrates is extremely important to reduce costs in analyte detection applications. As such, the reusability of flower-like Ag@MIPs was further investigated and the results are shown in Fig. 7, where it can be seen that although the SERS intensity of glibenclamide was detected to be slightly reduced in the process of reuse, the characteristic peaks of glibenclamide were still obvious. The reusability experiments indicated that the flower-like Ag@MIPs can be reused at least four times for the detection of glibenclamide. After several repeated uses, the SERS intensity of glibenclamide could still reach over 87% of the initial value. These results demonstrated that the flower-like Ag@MIPs as the SERS substrate exhibitedsatisfactory reusability and excellent stability.

The SERS enhancement mechanism of flower-like Ag@MIPs

In general, SERS enhancement is based on the combination of the electromagnetic effect and the chemical effect. The flower-like Ag was fabricated by the self-assembly of Ag nano-sheets. This geometrically complex system produces strong electromagnetic field coupling and can cause a strong SERS effect. The surface of the flower-like Ag was coated with an imprinted layer, and the thickness of the imprinted layer influenced the SERS enhancement. However, because of a large number of cavities in the imprinted layer, the flower-like Ag@MIPs maintained the excellent SERS enhancement performance. SERS hot spots were utilized to explain the SERS enhancement phenomenon. Hot spots were generated at special locations and SERS signals were greatly enhanced at the nanogaps and/or junctions between the metal particles and metal structures.[38,43,44] A small portion of template molecules contributed significant SERS enhancement at the hot spots.[45] Based on the above viewpoint, the possible reason for SERS enhancement in flower-like Ag@MIPs was that the surface molecular imprinting mainly occurs at plasmon hot spots.[46] In order to prove this assumption, Raman mapping images of flower-like Ag and Ag@MIPs were obtained at the characteristic peaks of 926 cm^{-1} and 1592 cm^{-1}, respectively. Hot spots were clearly observed as shown in Fig. 8. Compared with the Raman mapping images of flower-like Ag, the Raman mapping images of flower-like Ag@MIPs possessed more hot spots. The results showed that the intensity of Raman mapping at 1592 cm^{-1} was stronger than that at 926 cm^{-1}, which corresponds to the SERS spectra. Therefore, the SERS enhancement comes from the imprinted layer and not just the nanostructure plasmon resonance. Another reason was that the SERS enhancement originates from template molecule, due to the cavities in the imprinted layer specifically adsorbing the template molecules. Thus, the ratio of signal-to-noise was increased and caused the SERS enhancement. To sum up, the SERS enhancement of flower-like Ag@MIPs was attributed to the synergistic effect of electromagnetic enhancement and chemical enhancement.

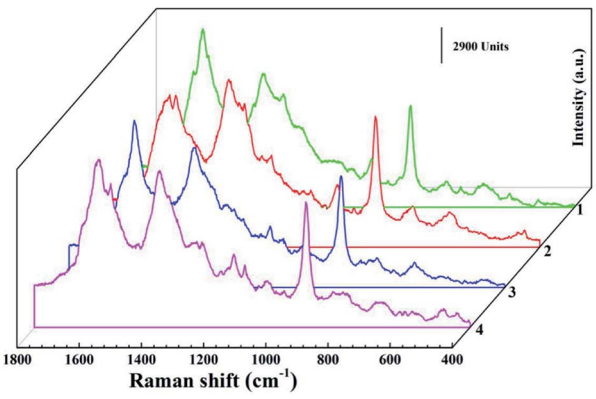

Fig. 7 The SERS spectra of glibenclamide obtained from re-used flower-like Ag@MIPs.

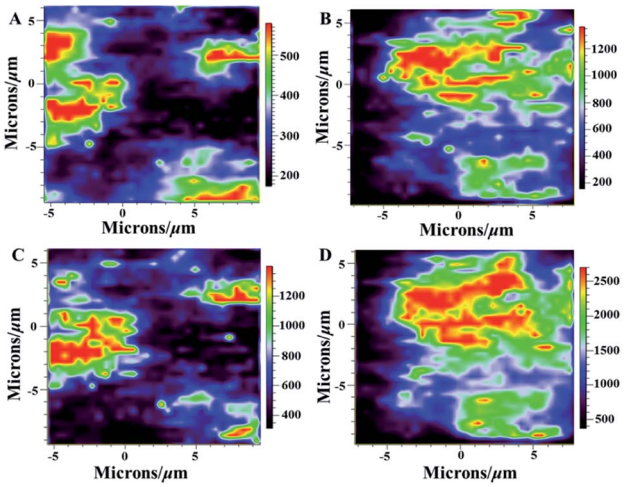

Fig. 8 The Raman mapping images of flower-like Ag (A and C), and Ag@MIPs (B and D) (the characteristic peaks at 926 cm^{-1} (A and B) and 1592 cm^{-1} (C and D)).

Conclusion

Based on the combination of SERS with high sensitivity and MIPs with excellent selectivity, flower-like Ag@MIPs were developed as an effective analytical technique for the detection of glibenclamide. The flower-like Ag@MIPs were prepared with the MIPs shell being less than 12 nm and the minimum detectable concentration of glibenclamide was down to 1 ng mL^{-1}. The specific recognition experiments indicated that the

flower-like Ag@MIPs as the SERS substrate exhibited stronger SERS enhancement for glibenclamide as compared to metformin hydrochloride. The reusability results of flower-like Ag@MIPs demonstrated that after being reused four times, the SERS intensity of glibenclamide could still retain 87% of the initial value. The significant SERS enhancement was put down to the combination of the electromagnetic and chemical effects. Although the flower-like Ag@MIPs possess outstanding selectivity, excellent stability and satisfactory sensitivity, there are still some problems with practical application, so further improvements will be continually made.

Conflicts of interest

There are no conflicts to declare.

Acknowledgements

We are grateful for the financial support of this research from the National Natural Science Foundation of China (51779065), and State Key Laboratory of Urban Water Resource and Environment, Harbin Institute of Technology (2019DX11).

Notes and references

1 A. Bari, N. Chella, K. Sanka, N. R. Shastri and P. V. Diwan, *J. Microencapsul.*, 2015, **32**, 54–60.
2 L. Yu, C. X. Li, Y. Le, J. F. Chen and H. K. Zou, *Mater. Chem. Phys.*, 2011, **130**, 361–366.
3 N. Haq, F. K. Alanazi, I. A. Alsarra and F. Shakeel, *Iran. J. Pharm. Res.*, 2014, **13**, 863–872.
4 A. N. Hasanah, F. Pessagno, R. E. Kartasasmita, S. Ibrahima and P. Manesiotis, *J. Mater. Chem. B*, 2015, **3**, 8577–8583.
5 N. Li, Y. Deng, D. Wang, Y. Qiao and F. M. Li, *Talanta*, 2013, **104**, 109–115.
6 M. Gazizadeh, G. Dehghan and M. Amjadi, *Luminescence*, 2019, **34**, 297–303.
7 P. Hartvig, C. Fagerlund and O. Gyllenhaal, *J. Chromatogr.*, 1980, **181**, 17–27.
8 V. Maier, J. Znaleziona, D. Jirovský, J. Skopalová, J. Petr and J. Ševčík, *J. Chromatogr. A*, 2009, **1216**, 4492–4498.
9 M. J. Bogusz, H. Hassan, E. Al-Enazi, Z. Ibrahim and M. Al-Tufail, *J. Pharmaceut. Biomed. Anal.*, 2006, **41**, 554–564.
10 K. S. Lakshmi and T. Rajesh, *J. Iran. Chem. Soc.*, 2011, **8**, 31–37.
11 S. Pang, T. X. Yang and L. L. He, *TrAC, Trends Anal. Chem.*, 2016, **85**, 73–82.
12 S. Suzuki, *e-J. Surf. Sci. Nanotechnol.*, 2019, **17**, 71–82.
13 K. Kneipp, Y. Wang, H. Kneipp, L. T. Perelman, I. Itzkan, R. R. Dasari and M. S. Feld, *Phys. Rev. Lett.*, 1997, **78**, 1667–1670.
14 S. Nie and S. R. Emory, *Science*, 1997, **275**, 1102–1106.
15 D. D. Huang, J. C. Zhao, M. L. Wang and S. H. Zhu, *Food Contr.*, 2020, **108**, 106835–106841.
16 B. B. Nie, Y. Y. Luo, J. P. Shi, L. Gao and G. T. Duan, *Sens. Actuators, B*, 2019, **301**, 127087–127095.
17 R. Wang, L. P. Zhang, S. Y. Zou and H. Zhang, *Microchem. J.*, 2019, **150**, 104127–104131.
18 S. Y. Liu, Q. Q. Chen, Z. M. Wang, T. C. Cao, G. H. Zhao and Y. X. Zhou, *Analyst*, 2019, **144**, 4841–4847.
19 J. W. Wu, L. X. Zhang, X. F. Bu, P. Li, B. Zhao and Y. Tian, *Analyst*, 2018, **143**, 5202–5209.
20 J. W. Wu, H. Ma, X. F. Bu, C. Ma, L. Zhu, B. Q. Hao, B. Zhao and Y. Tian, *Microchim. Acta*, 2019, **186**, 801–810.
21 S. Hu, Y. Gao, Y. P. Wu, X. Y. Guo, Y. Ying, Y. Wen and H. F. Yang, *Biosens. Bioelectron.*, 2019, **129**, 24–28.
22 J. F. Li, Y. F. Huang, Y. Ding, Z. L. Yang, S. B. Li, X. S. Zhou, F. R. Fan, W. Zhang, Z. Y. Zhou, D. Y. Wu, B. Ren, Z. L. Wang and Z. Q. Tian, *Nature*, 2010, **464**, 392–395.
23 A. S. D. S. Indrasekara, R. Thomasa and L. Fabris, *Phys. Chem. Chem. Phys.*, 2015, **17**, 21133–21142.
24 Y. Guo, L. L. Kang, S. N. Chen and X. Li, *Phys. Chem. Chem. Phys.*, 2015, **17**, 21343–21347.
25 S. Han, X. Li, Y. Wang and S. N. Chen, *Chem. Eng. J.*, 2015, **271**, 87–95.
26 H. He, P. Muhammad, Z. C. Guo, Q. L. Peng, H. F. Lu and Z. Liu, *Biosens. Bioelectron.*, 2019, **146**, 111733.
27 M. V. Polyakov, *Zh. Fiz. Khim.*, 1931, **2**, 799–805.
28 C. Alexander, H. S. Andersson, L. I. Andersson, R. J. Ansell, N. Kirsch, I. A. Nicholls, J. O' Mahony and M. J. Whitcombe, *J. Mol. Recognit.*, 2006, **19**, 106–180.
29 S. Han, X. Li, Y. Wang and C. Su, *Anal. Methods*, 2014, **6**, 2855–2861.
30 G. Wulff, *Angew. Chem., Int. Ed. Engl.*, 1995, **34**, 1812–1832.
31 K. Mosbach, *Trends Biochem. Sci.*, 1994, **19**, 9–14.
32 F. Gao, Y. X. Hu, D. Chen, E. C. Y. Li-Chan, E. Grant and X. N. Lu, *Talanta*, 2015, **143**, 344–352.
33 H. J. Li, Z. R. Wang, X. N. Wang, J. Q. Jiang, Y. Q. Xu, X. Q. Liu, Y. S. Yan and C. X. Li, *Anal. Bioanal. Chem.*, 2017, **409**, 4627–4635.
34 Z. W. Wang, R. X. Yan, S. W. Liao, Y. R. Miao, B. Zhang, F. Wang and H. F. Yang, *Appl. Surf. Sci.*, 2018, **457**, 323–331.
35 S. L. Feng, Y. X. Hu, L. Y. Ma and X. N. Lu, *Sens. Actuators, B*, 2017, **241**, 750–757.
36 B. W. Zhao, S. L. Feng, Y. X. Hua, S. Wang and X. N. Lu, *Food Chem.*, 2019, **276**, 366–375.
37 R. R. Xing, Y. R. Wen, Y. R. Dong, Y. J. Wang, Q. Zhang and Z. Liu, *Anal. Chem.*, 2019, **91**(15), 9993–10000.
38 X. H. Ren, L. Yang, Y. C. Li, E. C. Cheshari and X. Li, *Spectrochim. Acta, Part A*, 2020, **228**, 117764–117772.
39 L. L. Zhou, Y. J. Wang, R. R. Xing, J. Chen, J. Liu, W. Li and Z. Liu, *Biosens. Bioelectron.*, 2019, **145**, 111729.
40 J. Liu, D. Y. Yin, S. S. Wang, H. Y. Chen and Z. Liu, *Angew. Chem.*, 2016, **55**, 13215–13218.
41 X. H. Ren, E. C. Cheshari, J. Y. Qi and X. Li, *Microchim. Acta*, 2018, **185**, 242–249.
42 L. Wang, H. L. Li, J. Q. Tian and X. P. Sun, *ACS Appl. Mater. Interfaces*, 2010, **2**, 2987–2991.
43 M. Rycenga, X. H. Xia, C. H. Moran, F. Zhou, D. Qin, Z. Y. Li and Y. N. Xia, *Angew. Chem.*, 2011, **123**, 5587–5591.
44 K. Qian, H. L. Liu, L. B. Yang and J. H. Liu, *Nanoscale*, 2012, **4**, 6449–6454.
45 Y. Fang, N. H. Seong and D. D. Dlott, *Science*, 2008, **321**, 388–392.
46 A. Abbas, L. M. Tian, J. J. Morrissey, E. D. Kharasch and S. Singamaneni, *Adv. Funct. Mater.*, 2013, **23**, 1789–1797.